Supporting Information

Giometto et al. 10.1073/pnas.1321167110

Experiments

1.1. Dispersal Experiment. Density profiles in the six replicated dispersal events, at successive times, are shown in Fig. 2 *A–F*. Collected data were binned in 5-cm bins, which corresponds to the typical length scale of the dispersal process ($\sqrt{D/r} \simeq 5$ cm). Individuals of *Tetrahymena* sp., initially localized at one end of the landscape, colonized the whole system in 4 d. The position of the wavefront at each time was estimated by looking for the first occurrence, starting from the end of the landscape, of a fixed value of the density (more precisely, we linearly interpolated the density profile between the first occurrence of a density value above threshold and the following spatial point), which we set at $\rho^\star = 200$ ind/cm (results are not affected by different choices of this reference value) (Fig. 3*C*). The position of the wavefront at different times is shown in Fig. 3*A*. As noticeable, there is an initial growth phase followed by a linear increase in the front's coordinate with time. We fitted a linear model (least-squares fit) to each replica in the linear region (1–4 d) and found a mean speed of $v_o = 52.0 \pm 1.8$ cm/d (mean ± SE). Note that the existence of an initial nonlinear spread has been documented in several case studies (1–3). Shown in Table S1 are the observed velocities in the six replicas (Fig. 3).

1.2. Local Growth Experiment. We discuss here the analysis of growth measurements according to the deterministic framework of the Fisher–Kolmogorov equation. For the analysis of these data in the stochastic framework, see section 2.2.

We report in Table S2 the best-fit parameters of the deterministic logistic model $d\rho/dt = r\rho[1-\rho/K]$ to the growth measurements data. Note that the variability in the carrying capacity among replicas resembles the variability in the mean density observed in the dispersal experiment in the region behind the wavefront (Fig. 2).

1.3. Local Movement Experiment. We ran four additional dispersal events, independent from the dispersal experiment, and recorded videos of individuals moving ahead of the advancing wavefront, where the density was low. To obtain experimental estimates of the diffusion coefficient, we fitted the measured values of $\langle x^2(t)\rangle$ to the equation $\langle x^2(t)\rangle = 2Dt - 2D\tau[1-e^{-t/\tau}]$, for all videos of each replica (see section 4.2.1 for a derivation of this equation in the context of persistent random walks). The mean value of the diffusion coefficient is $D = 0.17 \pm 0.01$ mm^2/s $= 140 \pm 10$ cm^2/d; the mean autocorrelation time is $\tau = 3.9 \pm 0.4$ s.

Note that we have measured the diffusion coefficient by looking at individuals at the front of the traveling wave, as these are the individuals responsible for the colonization of empty space. During the dispersal experiment, we also measured the diffusion coefficient of *Tetrahymena* sp. in the bulk of the wave, that is, where the population was at high density. We observed that trajectories differ qualitatively between the bulk and the front of the wave, and this difference reflects in a much smaller diffusion coefficient estimate where the population is at carrying capacity. In fact, in the bulk of the wave, we measured a mean diffusion coefficient of $D_{bulk} = 0.003 \pm 0.001$ mm^2/s, much smaller than at the wavefront. Such density-dependent effects, however, are not assumed to be operating at the low densities that determine the speed of the front, and the results support our assumption.

1.4. Speed of the Wavefront: Deterministic Prediction and Observations. Here, we compare the wavefront speeds observed in the dispersal experiment to predictions of the theory (deterministic Fisher–Kolmogorov Eq. **1**) (*Materials and Methods*), for which we use the independent estimates of r and D (as in sections 1.2 and 1.3). Use of the mean value of $r = 4.9 \pm 0.5$ d^{-1} (mean ± SE) and $D = 140 \pm 10$ cm^2/d (mean ± SE) gives a predicted speed of $v_{FK} = 2\sqrt{rD} = 52.4 \pm 3.3$ cm/d. In the main text, we adopted a bootstrap approach and computed the quantity $2\sqrt{rD}$ for all possible combinations of the r and D values measured in the growth and movement experiments. The mean speed computed with this approach is $v = 51.9 \pm 1.1$ cm/d (mean ± SE). Both v_{FK} and v are very close and compatible with the mean observed speed in the dispersal experiment, $v_o = 52.0 \pm 1.8$ cm/d (mean ± SE). To further compare the predicted values for the speed in the bootstrap approach to the observed speed in the dispersal experiment, we performed a t test between the two sets. The t test gives a P value $p = 0.96$ ($t = 0.05$, $df = 9$); thus, the null hypothesis that the mean difference is 0 is not rejected at the 5% level. Therefore, there is no indication that the two means are different.

Stochastic Model

The Fisher–Kolmogorov Eq. **1** (*Materials and Methods*) is deterministic and therefore cannot reproduce the variability observed in biological dispersal (4) (Fig. 3). To address fluctuations in the range expansion of invading species, we propose a stochastic partial differential equation (SPDE), that is, a generalization of Eq. **1**, accounting for demographic stochasticity. The SPDE reads:

$$\frac{\partial \rho}{\partial t} = D\frac{\partial^2 \rho}{\partial x^2} + r\rho\left[1-\frac{\rho}{K}\right] + \sigma\sqrt{\rho}\eta, \qquad \textbf{[S1]}$$

where η is a Gaussian, zero-mean white noise [i.e., $\langle \eta(x,t)\,\eta(x',t')\rangle = \delta(x-x')\delta(t-t')$, with δ the Dirac's delta function] and $\sigma > 0$ measures the noise strength. We adopt the Itô's stochastic calculus (5), as appropriate in this case. Note, in fact, that the choice of the Stratonovich framework would make no sense here, as the noise term would have a constant nonzero mean (5, 6), which would allow an extinct population to possibly escape the zero-density absorbing state. We simulated Eq. **S1** using the estimates for r, K, and σ obtained with a maximum likelihood approach applied to the growth experiment data (section 2.2) and D as estimated in the local movement experiment (section 1.3). The square-root multiplicative noise term in Eq. **S1** is commonly interpreted as describing demographic stochasticity in a population (7) and needs extra care in simulations (8, 9). In particular, standard stochastic integration schemes fail to preserve the positivity of ρ. We adopted a recently developed split-step method (9) (see also section 2.1) to numerically integrate Eq. **S1**. This method allows us to perform the integration with relatively large spatial and temporal steps maintaining numerical accuracy. Fig. 2 *G* and *H* shows two integrations of Eq. **1** with initial conditions as in Fig. 2 *A* and *B* at the second experimental time point. Simulations were performed with reflective boundary conditions at $x = 0$ cm and $x = 220$ cm and with the parameters $r = 6.1$ d^{-1}, $K = 903$ ind/cm, $\sigma = 25$ d$^{-\frac{1}{2}}$ (results of the maximum likelihood estimation) (see section 2.2) and $D = 140$ cm^2/d. The integration steps were $\Delta x = 5$ cm and $\Delta t = 0.002$ d, which were able to reproduce the deterministic behavior and speed for very small values of the noise strength σ. It should be noted that the mathematical structure of Eq. **S1** allows the formation of traveling waves, although endowed with a speed slower than $2\sqrt{rD}$. The reader is referred to the literature for a detailed account of the mathematical details (6, 10, 11). Suffice it here to note that the parameter identification of the

demographic traits r, K, and σ on the growth experiment data accounts for the relative balance of the processes and results in a reliable prediction of both the mean speed and the range variability (section 2.3).

2.1. Spatial Discretization. Eq. **S1** is interpreted as the continuum limit of a set of coupled Itô equations resulting from a discretization of space (9). Let Δx be the step of spatial discretization on a $1D$ lattice. The discretization reads:

$$\frac{d\rho_i}{dt}(t) = \frac{D}{(\Delta x)^2}\left[\rho_{i+1}(t) + \rho_{i-1}(t) - 2\rho_i(t)\right] + \\ + r\rho_i(t)\left(1 - \frac{\rho_i(t)}{K}\right) + \frac{\sigma}{\sqrt{\Delta x}}\sqrt{\rho_i(t)}\eta(t), \qquad [S2]$$

where i identifies the lattice site and the term $\sqrt{\Delta x}$ ensures proper normalization in the continuum limit (12). This spatial discretization allows us to compare the noise term in Eq. **S1** to the local noise acting at a lattice site of size Δx. In particular, it allows us to estimate the noise strength σ by parameter identification on the growth experiment data, where we looked at the density of a single site i of size $l = 7$ cm (a length comparable with the step size adopted in the numerical integration, that is $\Delta x = 5$ cm). The equation governing the density of the single site i in the growth experiment is thus:

$$\frac{d\rho}{dt}(t) = r\rho(t)\left(1 - \frac{\rho(t)}{K}\right) + \frac{\sigma}{\sqrt{l}}\sqrt{\rho(t)}\eta(t), \qquad [S3]$$

where the diffusion term is neglected as we are in a well-mixed setting and we dropped the i subscript as we only have one site. The maximum likelihood approach described in the following section allows us to estimate r, K, and σ from the experimental growth data.

2.2. Parametric Inference in the Stochastic Framework. We fit Eq. **S3** to the growth data (local growth experiment), with fitting parameters r, K, and σ. The likelihood function for Eq. **S3** can be written as:

$$L(\theta) = \prod_{j=2}^{n} P\left[\rho(t_j), t_j | \rho(t_{j-1}), t_{j-1}; \theta\right], \qquad [S4]$$

where n is the total number of observations in the growth time series, $\theta = (r, K, \sigma)$ is the vector of demographic parameters, and $P(\rho, t|\rho_0, t_0; \theta)$ is the transitional probability density of having a density of individuals ρ at time t, given that the density at time t_0 was ρ_0 (for a given θ). The transitional probability density $P(\rho, t|\rho_0, t_0; \theta)$ satisfies the Fokker–Planck equation associated with Eq. **S3**, that is:

$$\frac{\partial}{\partial t}P(\rho, t|\rho_0, t_0; \theta) = -\frac{\partial}{\partial \rho}\left[r\rho\left(1 - \frac{\rho}{K}\right)P(\rho, t|\rho_0, t_0; \theta)\right] + \\ + \frac{\sigma^2}{2l}\frac{\partial^2}{\partial \rho^2}\left[\rho P(\rho, t|\rho_0, t_0; \theta)\right]. \qquad [S5]$$

Maximization of the likelihood is equivalent to the minimization of the negative log-likelihood $-\log L(\theta)$, which is computationally less expensive. To compute the likelihood for a fixed set of parameters θ, one has to solve numerically the Fokker–Planck Eq. **S5** for all observed transitions, with the $[t_j, \rho(t_j)]$ as measured in the experiment. It is computationally more accurate to solve Eq. **S5** in terms of the cumulative distribution function (CDF), as its initial condition in the transition $[t_{j-1}, \rho(t_{j-1})] \to [t_j, \rho(t_j)]$ can be expressed as a step function instead of a delta function, the first one being more accurate in the numerical approximation (13). The transitional probability densities (solutions of Eq. **S5**) can then be recovered by numerical differentiation. The numerical integration was performed adopting the implicit Crank–Nicolson scheme (13); the minimization was performed with the software *MATLAB*, adopting the active-set algorithm in a large domain. We verified that different initial conditions for the parameters led to the same estimate for the minimum, which is thus interpreted as the global minimum of the negative log-likelihood function, that is, the global maximum for the likelihood function. The set of demographic parameters that maximized the likelihood function is $r = 6.1 \pm 0.8$ d^{-1}, $K = 903 \pm 135$ ind/cm, $\sigma = 25 \pm 5$ d$^{-\frac{1}{2}}$ (mean ± SE).

2.3. Comparison with Experimental Data. ***Wavefront.*** The black curve in Fig. 3*A* is the mean position of the front over 1,020 integrations of Eq. **S1**, with 170 iterations starting from each experimental density profile at the second measurement time point (Fig. 3*A* and *Materials and Methods*). The dark and light gray shadings in Fig. 3*A* represent, respectively, the 95% and 99% intervals for the front's position. The increase in width for the front's position is captured by the red curve in Fig. 3*B*, which represents the 95% interval width for the front's position at each time step. Simulations are in quantitative agreement with data (Fig. 3*B*). Examples of the front's position in different simulations of the stochastic equation are shown in Fig. S2.

Speed of the front. We measured the speed of the front in the stochastic simulations by fitting the front's position at eight equally spaced time points in the time interval $[1 - 4]$ d, over 1,020 integrations of Eq. **S1**. The resulting mean speed of the front was 52.1 cm/d; the SD was 4.2 cm/d. The mean speed in the dispersal experiment was 52.0 cm/d, and the measured SD was 4.3 cm/d.

On the Diffusion Coefficient Estimates in Field Studies

In the literature, reaction–diffusion processes applied to ecological processes were sometimes criticized because of unsatisfactory fits to some empirical observations. For instance, reaction–diffusion models have been questioned for neglecting the fact that organisms move at a finite speed (3, 14) or for predicting slower spreads with respect to observations (3). The presence of rare long-distance dispersers has been invoked by some authors (1, 3) to account for the observation of faster-than-predicted spreads. We argue that the origins of some mismatches between empirical observations and reaction–diffusion models could be due to imprecise estimates of the diffusion coefficient, which proved to be the most delicate measurement also in our experiment. In fact, the diffusion coefficient is traditionally measured through the mean square displacement (MSD) of individuals or collective movement, computed with the available data. These data might refer to a timescale that is too short to be in the region of linear increase of MSD with time; that is, one might be still observing the autocorrelated phase that is shown in Fig. S1 for small times. Computing the MSD in the auto-correlated region leads to a lower estimate of the diffusion coefficient, which in turn leads to a smaller predicted speed for the advancing wavefront. When computing the MSD, therefore, one should compute it at different time points until the autocorrelated and linear regimes are discernible. Notably, the duration of the autocorrelated phase is expected to vary significantly from species to species (15). Additionally, our experiment supports that the diffusion coefficient estimate should be performed in density-independent conditions.

Theoretical Background

Reaction–diffusion models have been shown to accurately describe the spread of organisms in many comparative studies (1, 16, 17) and are here experimentally confirmed. We acknowledge that models other than reaction–diffusion equations, such as integro-difference equations involving dispersal kernels, are best suited to describe dispersal of organisms that exhibit distinct reproductive and dispersive phases (3, 4). However, for many organisms, especially those with continuous, nonoverlapping

generations and temporally unstructured dispersal–reproductive dynamics, the reaction–diffusion approach is highly appropriate (16–18). Refinements of reaction–diffusion models have also been put forward in the literature. For instance, reaction–telegraph models were introduced to account for the finite movement speed of individuals, resulting in a correction to the wavefront speed (14), which is, however, negligible for our study species, as we show in the following sections. Here, we briefly review the theoretical framework of reaction–diffusion processes and discuss the relationship to reaction–telegraph processes, with reference to our experiment. The interested reader can refer to specialized texts for further investigation and generalizations (5, 19, 20).

4.1. The Fisher–Kolmogorov Equation. ***4.1.1. Brownian motion and the mean square displacement of particles.*** The diffusion equation

$$\frac{\partial \rho}{\partial t}(x,t) = D\frac{\partial^2 \rho}{\partial x^2}(x,t) \qquad \textbf{[S6]}$$

describes the evolution of the density of an ensemble of independent random walkers (5). The diffusion coefficient D can be measured as the proportionality constant that links the mean square displacement to time as (5):

$$\langle x_t^2 \rangle = 2Dt, \qquad \textbf{[S7]}$$

with D as in Eq. **S6**.

4.1.2. Reaction–diffusion equations and the Fisher–Kolmogorov equation. Macroscopically, or phenomenologically, the continuity equation in the presence of a reaction term reads:

$$\frac{\partial \rho}{\partial t} = -\frac{\partial J}{\partial x} + F(\rho). \qquad \textbf{[S8]}$$

Assuming proportionality between the flux J and the density gradient $\partial\rho/\partial x$ via the diffusion coefficient, one finds the so-called reaction–diffusion equation (18, 20–22):

$$\frac{\partial \rho}{\partial t} = D\frac{\partial^2 \rho}{\partial x^2} + F(\rho). \qquad \textbf{[S9]}$$

If the reaction term $F(\rho)$ is logistic, one finds the Fisher–Kolmogorov equation:

$$\frac{\partial \rho}{\partial t} = D\frac{\partial^2 \rho}{\partial x^2} + r\rho\left[1 - \frac{\rho}{K}\right], \qquad \textbf{[S10]}$$

where ρ is the density of organisms, D is the diffusion coefficient of the species, r is its growth rate, and K its carrying capacity.

4.1.3. Traveling waves in the Fisher–Kolmogorov equation. The Fisher–Kolmogorov Eq. **S10** is probably the best known example of an equation that accepts traveling wave solutions. A traveling wave is a wave that travels without change of shape; that is, the density profile along a line moves rigidly in time without deformation (Fig. 1*E*). Mathematically, these dynamics of propagation mean that, if $u(x,t)$ is a traveling wave solution of a reaction–diffusion equation, then $u(x,t)$ is a function of $x - vt$, where v is the speed of the wave; that is, $u(x,t) = u(x - vt)$.

Dimensional analysis of Eq. **S10** shows that the speed is $v \propto \sqrt{rD}$. Fisher (21) proved that traveling wave solutions can only exist with speed $v \geq 2\sqrt{rD}$ and Kolmogorov (22) demonstrated that, with suitable and reasonable initial conditions, the verified speed of the wavefront is equal to the lower bound; that is,

$$v = v_{FK} = 2\sqrt{rD}. \qquad \textbf{[S11]}$$

For any concave $F(\rho)$ in Eq. **S9**, that is, $F(\rho) \leq \rho F'(0)$, the front velocity has been shown to be equal to $v_{RD} = 2\sqrt{DF'(0)}$ (20). The interested reader can refer to the original works by Fisher (21) and Kolmogorov (22) or read one of the many good books on the topic (18, 20).

4.2. The Reaction–Telegraph Equation. The diffusion equation has been widely used to describe the movement of organisms (2, 18). It is clear, however, that individuals do not perform exact random walks at the microscopic scale (where "microscopic" here is used to refer to the typical length scale of an organism). What is implied when adopting diffusion equations to describe movement behaviors is that there exists an appropriate mesoscopic scale in which the collective behavior of organisms is indistinguishable from that of an ensemble of random walkers (1). In this section, we justify why the adoption of a reaction–diffusion equation is appropriate for our system, which follows from the fact that the correlation time in the trajectories performed by individuals of the species *Tetrahymena* sp. is much smaller than the typical timescale of the dispersal process or, more precisely, the growth rate of the species (Eq. **S19**).

4.2.1. Persistent random walk. One can describe the movement of an individual (particle) as a sequence of jumps of length Δx and duration Δt. A model for a correlated random walk was introduced by R. Fürth (23) and assumes that particles move along an infinite line at a constant speed γ, with a probability μ per unit time to reverse its direction of motion. Precisely, the probability for the particle to continue in the direction of motion is given by $1 - \mu\Delta t$ and the probability to reverse its direction is $\mu\Delta t$, in such a way that the speed $\lim_{\Delta x, \Delta t \to 0} \Delta x/\Delta t = \gamma$ is constant.

With these assumptions (20) one obtains the telegraph equation for the density of particles:

$$\frac{1}{2\mu}\frac{\partial^2 \rho}{\partial t^2} + \frac{\partial \rho}{\partial t} = \frac{\gamma^2}{2\mu}\frac{\partial^2 \rho}{\partial x^2}, \qquad \textbf{[S12]}$$

which we rewrite as

$$\tau\frac{\partial^2 \rho}{\partial t^2} + \frac{\partial \rho}{\partial t} = D\frac{\partial^2 \rho}{\partial x^2}, \qquad \textbf{[S13]}$$

where $\tau^{-1} = 2\mu$ is the correlation time of the turning process and $D = \gamma^2/(2\mu)$. Note that Eq. **S13** differs from the diffusion equation for the additional term $\tau\frac{\partial^2 \rho}{\partial t^2}$. Eq. **S13** is a hyperbolic equation, and therefore information cannot travel faster than the speed of particles γ. In a way, then, the telegraph equation is physically more appropriate than the diffusion equation, as for the diffusion equation the probability density of finding a particle in an infinitesimal interval around (x,t) is larger then zero for all x and $t > 0$; that is, signals can travel at infinite speed. In our specific case, the correlation time τ is very small, so we argue that the term $\tau\frac{\partial^2 \rho}{\partial t^2}$ is negligible compared with the other terms in the equation, and thus the system is well-described by the diffusion equation. To estimate the parameters τ and D from experimental data, one can compute the value for the mean square displacement along the line, that is,

$$\langle x^2 \rangle = \int_{-\infty}^{+\infty} dx\, x^2 \rho(x,t). \qquad \textbf{[S14]}$$

Multiplying Eq. **S13** by x^2 and integrating one has

$$\tau\int_{-\infty}^{+\infty} dx\, x^2 \frac{\partial^2 \rho}{\partial t^2}(x,t) + \int_{-\infty}^{+\infty} dx\, x^2 \frac{\partial \rho}{\partial t}(x,t) = D\int_{-\infty}^{+\infty} dx\, x^2 \frac{\partial^2 \rho}{\partial x^2}(x,t), \qquad \textbf{[S15]}$$

which reads

$$\tau \frac{d^2\langle x^2\rangle}{dt^2} + \frac{d\langle x^2\rangle}{dt} = 2D, \qquad \textbf{[S16]}$$

assuming that $\rho(x,t)$, $\frac{\partial\rho}{\partial t}(x,t)$ and $\frac{\partial^2\rho}{\partial t^2}(x,t)$ go to zero sufficiently fast for $x \to \pm\infty$. Assuming further that $\rho(x,0) = \delta(x)$ (where δ is the delta function) and $\partial p/\partial t(x,t)|_{t=0} = 0$, one has $\langle x^2\rangle|_{t=0} = d\langle x^2\rangle/dt|_{t=0} = 0$ and

$$\langle x^2(t)\rangle = 2Dt - 2D\tau\left[1 - e^{-t/\tau}\right]. \qquad \textbf{[S17]}$$

Fig. S1 shows that Eq. **S17** provides a very good fit to the experimentally measured mean square displacement for individuals of *Tetrahymena* sp.

4.2.2. The reaction–telegraph equation. One can amend the instantaneous adjustment of the flux to the density gradient implied by Fick's first law with the introduction of a relaxation time τ, which leads to the reaction–telegraph equation (14, 20)

$$\tau\frac{\partial^2\rho}{\partial t^2} + \left[1 - \tau F'(\rho)\right]\frac{\partial\rho}{\partial t} = D\frac{\partial^2\rho}{\partial x^2} + F(\rho). \qquad \textbf{[S18]}$$

Eq. **S18** can be obtained combining the telegraph Eq. **S13** with kinetics (20). Eq. **S18** differs from the reaction–diffusion Eq. **S9** for the additional term $\tau\frac{\partial^2\rho}{\partial t^2} - \tau F'(\rho)\frac{\partial\rho}{\partial t}$. Solutions of Eq. **S18** converge to solutions of the reaction–diffusion equation as $\tau \to 0$ (20, 24). In our case, we argue that the correlation time τ is sufficiently small to consider the process as well described by the reaction–diffusion equation. We will give quantitative support to this statement in the next section. One can also show that the introduction of reactions in the persistent random-walk equations leads to the reaction–telegraph Eq. **S18** (20) with $\tau^{-1} = 2\mu$ and $D = \gamma^2/(2\mu)$ as in Eq. **S13**.

4.2.3. Traveling waves in the reaction–telegraph equation. E. E. Holmes (14) studied the propagation of traveling wavefronts in the reaction–telegraph equation with logistic reaction F, estimating model parameters for several case studies. The reaction–telegraph Eq. **S18** with logistic growth was shown (25) to accept traveling wave solutions with speed:

$$v_{RT} = \frac{2\sqrt{rD}}{1+\tau r} = \frac{v_{FK}}{1+\tau r} \qquad \textbf{[S19]}$$

if $r\tau < 1$; otherwise $v_{RT} = (D/\tau)^{\frac{1}{2}}$. In this perspective, we claim that, in our specific case, the ratio between the speed of a reaction–telegraph and that of a reaction–diffusion equation is practically one. In fact, we find $r\tau = (2.2 \pm 0.3)\cdot 10^{-4}$ so that $v_{RT}/v_{RD} > 0.999$, which makes the two processes experimentally undistinguishable. Therefore, we conclude that our system is well-described by Eq. **1** (*Materials and Methods*), and this agreement with the Fisher–Kolmogorov equation is due to the very small value of the correlation time τ with respect to the growth rate r.

1. Andow DA, Kareiva PM, Levin SA, Okubo A (1990) Spread of invading organisms. *Landscape Ecol* 4(2/3):177–188.
2. Okubo A, Levin SA (2002) *Diffusion and Ecological Problems: Modern Perspectives* (Springer, Berlin), 2nd Ed.
3. Hastings A, et al. (2005) The spatial spread of invasions: New developments in theory and evidence. *Ecol Lett* 8(1):91–101.
4. Melbourne BA, Hastings A (2009) Highly variable spread rates in replicated biological invasions: fundamental limits to predictability. *Science* 325(5947):1536–1539.
5. Gardiner C (2006) *Stochastic Methods* (Springer, Berlin), 4th Ed.
6. Méndez V, Llopis I, Campos D, Horsthemke W (2011) Effect of environmental fluctuations on invasion fronts. *J Theor Biol* 281(1):31–38.
7. Bonachela J, Muñoz MA, Levin SA (2012) Patchiness and demographic noise in three ecological examples. *J Stat Phys* 148(4):723–739.
8. Moro E (2004) Numerical schemes for continuum models of reaction-diffusion systems subject to internal noise. *Phys Rev E Stat Nonlin Soft Matter Phys* 70(4 Pt 2): 045102.
9. Dornic I, Chaté H, Muñoz MA (2005) Integration of Langevin equations with multiplicative noise and the viability of field theories for absorbing phase transitions. *Phys Rev Lett* 94(10):100601.
10. Moro E (2001) Internal fluctuations effects on Fisher waves. *Phys Rev Lett* 87(23): 238303.
11. Hallatschek O, Korolev KS (2009) Fisher waves in the strong noise limit. *Phys Rev Lett* 103(10):108103.
12. Doering CR, Sargsyan KV, Smereka P (2005) A numerical method for some stochastic differential equations with multiplicative noise. *Phys Lett A* 344(2/4):149–155.
13. Hurn AS, Jeisman JI, Lindsday KA (2007) Transitional densities of diffusion processes: A new approach to solving the Fokker-Planck equation. *J Deriv* 14(4):86–94.
14. Holmes EE (1993) Are diffusion models too simple? A comparison with telegraph models of invasion. *Am Nat* 142(5):779–795.
15. Li L, Nørrelykke SF, Cox EC (2008) Persistent cell motion in the absence of external signals: A search strategy for eukaryotic cells. *PLoS ONE* 3(5):e2093.
16. Lubina JA, Levin SA (1988) The spread of a reinvading species: Range expansion in the California sea otter. *Am Nat* 131(4):526–543.
17. Grosholz ED (1996) Contrasting rates of spread for introduced species in terrestrial and marine systems. *Ecology* 77(6):1680–1686.
18. Murray JD (2004) *Mathematical Biology I: An Introduction* (Springer, Berlin), 3rd Ed.
19. Berg HC (1993) *Random Walks in Biology* (Princeton Univ Press, Princeton).
20. Méndez V, Fedotov S, Horsthemke W (2010) *Reaction-Transport Systems* (Springer, Berlin).
21. Fisher RA (1937) The wave of advance of advantageous genes. *Ann Eugen* 7:355–369.
22. Kolmogorov AN, Petrovskii IG, Piskunov NS (1937) A study of the diffusion equation with increase in the amount of substance, and its application to a biological problem. *Bull. Moscow Univ. Math. Mech.* 1(1):1–25.
23. Fürth R (1920) Die Brownsche Bewegung bei Berücksichtigung einer Persistenz der Bewegungsrichtung. Mit Anwendungen auf die Bewegung lebender Infusorien. *Z Phys* 2(3):244–256.
24. Zauderer E (1989) *Partial Differential Equations of Applied Mathematics* (Wiley, New York), 2nd Ed.
25. Méndez V, Camacho J (1997) Dynamics and thermodynamics of delayed population growth. *Phys Rev E Stat Phys Plasmas Fluids Relat Interdiscip Topics* 55(6):6476–6482.

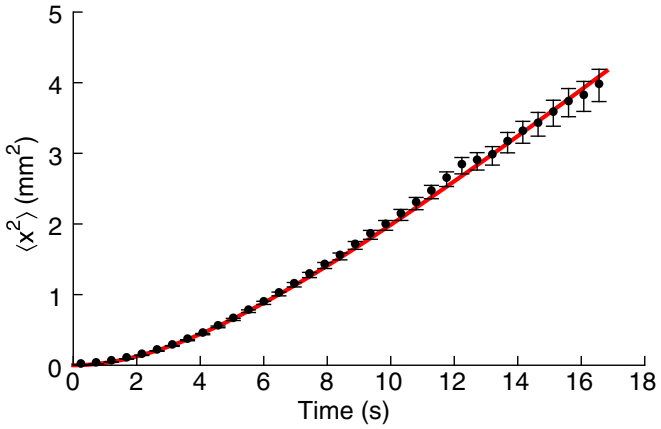

Fig. S1. Mean square displacement $\langle x^2 \rangle$ of individuals' trajectories versus time, for a representative video. The red curve is the best fit of the data to the equation $\langle x^2(t) \rangle = 2Dt - 2D\tau[1 - e^{-t/\tau}]$. After an initial auto-correlated phase, the mean square displacement increases linearly with time. Error bars are ± SE.

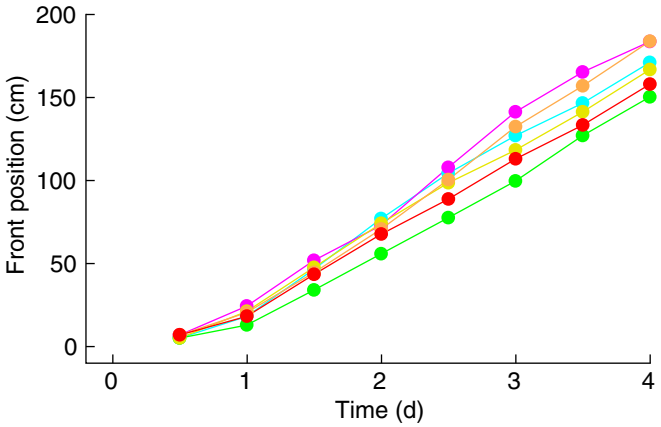

Fig. S2. Front's position in six integrations of the stochastic model Eq. **S1** (compare with experimental positions in Fig. 3*A*). Each simulation was initialized from each of the measured density profiles at the second experimental time point.

Table S1. Best-fit estimates of the wavefront speed in six replicated dispersal events

Replica	Speed, cm/d
1	54.6 ± 1.9
2	51.7 ± 2.8
3	48.0 ± 1.5
4	58.0 ± 4.0
5	53.4 ± 1.8
6	46.3 ± 1.0

Errors are ± SE.

Table S2. Best-fit estimates of the growth rate *r* and the carrying capacity *K* for *Tetrahymena* sp.

Replica	r, d^{-1}	K, ind/cm
1	6.0 ± 0.2	1020 ± 20
2	3.7 ± 0.2	680 ± 30
3	3.8 ± 0.5	950 ± 80
4	5.2 ± 0.7	550 ± 30
5	5.8 ± 0.5	1300 ± 92

Estimates of growth rate r and carrying capacity K obtained in five independent growth measurements. The fit is performed in the framework of the deterministic logistic equation. ind, individuals. Errors are $\pm$ SE.

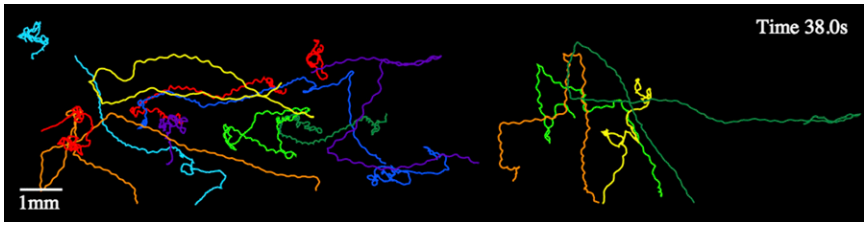

Movie S1. Reconstructed trajectories of individuals of *Tetrahymena* sp. swimming in density-independent conditions at the front of a traveling wave. Different colors identify different individuals.

Movie S1